Bioorganic & Medicinal Chemistry Letters 21 (2011) 1248–1252

Contents lists available at ScienceDirect

Bioorganic & Medicinal Chemistry Letters

journal homepage: www.elsevier.com/locate/bmcl

The Discovery of furo[2,3-*c*]pyridine-based indanone oximes as potent and selective B-Raf inhibitors

Alex J. Buckmelter [a], Li Ren [a,*], Ellen R. Laird [a,*], Bryson Rast [a], Greg Miknis [a], Steve Wenglowsky [a], Stephen Schlachter [a], Mike Welch [a], Eugene Tarlton [a], Jonas Grina [a], Joseph Lyssikatos [b], Barbara J. Brandhuber [a], Tony Morales [a], Nikole Randolph [a], Guy Vigers [a], Matthew Martinson [a], Michele Callejo [a]

[a] *Array BioPharma, 3200 Walnut Street, Boulder, CO 80301, United States*
[b] *Genentech, Inc., 1 DNA Way, South San Francisco, CA 94080-4990, United States*

ARTICLE INFO

Article history:
Received 18 October 2010
Revised 2 December 2010
Accepted 6 December 2010
Available online 10 December 2010

Keywords:
B-Raf
Kinase
Cancer therapy

ABSTRACT

Virtual and high-throughput screening identified imidazo[1,2-*a*]pyrazines as inhibitors of B-Raf. We describe the rationale, SAR, and evolution of the initial hits to a series of furo[2,3-*c*]pyridine indanone oximes as highly potent and selective inhibitors of B-Raf.

The Ras/Raf/MEK/ERK signal transduction pathway is critical to the survival, growth, and proliferation of cells and has been implicated in several human cancers. B-Raf is a serine-threonine kinase in this pathway that has been shown to have a much higher basal kinase activity relative to either of its isoforms (A-Raf or C-Raf), and recently has been reported to be frequently mutated in various human cancers. Activating B-Raf mutations, most notably V600E (formerly termed V599E), have been identified in 66% of melanomas and to lesser extents in many other cancers.[1] The Raf kinase inhibitor Bay 43-9006 (Sorafinib) has been approved for the treatment of renal cell carcinoma. However, its lack of activity in tumors that express mutant B-Raf, for example, melanoma, may arise because the principal mechanism of action is through inhibition of VEGFR rather than Raf.[2] The development of specific B-Raf inhibitors is therefore an active area of investigation for cancer therapy.

At the outset of this work in 2003, X-ray crystal structures of B-Raf were not available, although diverse inhibitor classes had been reported (Fig. 1). The triaryl imidazoles represented by L-779,450[3] are compact structures that possess very few conformations that could comprise the binding mode. A shape-based virtual screen of our in-house compound collection using the ROCS program[4] yielded 270 hits, the most interesting of which came from a library of imidazo[1,2-*a*]pyrazines[5] depicted in Figure 2. Subsequent screening confirmed compound **1a** (Table 1) as a 1.4 μM inhibitor.[6] Because acylated and sulfonylated amines from the library were not active (data not shown), we anticipated that the aminomethylphenyl group was occupying a confined space.

Homology models of B-Raf were constructed on the basis of sequence similarity to the Src and MAP kinase families,[7] and confirmed that B-Raf possesses a small gatekeeper residue (Thr529), which is indicative of sensitivity to aryl substituents.[8] In order to differentiate between the possible binding modes (Fig. 3), a small set of analogs was synthesized (exemplified by compounds **1b** and **1c**, Table 1). In order to enhance hydrophobic contact in the pocket made accessible by the gatekeeper threonine (the 'gatekeeper pocket'), the 4-aminomethyl group was replaced with 4-chloro, which led to a modest improvement in activity. Subsequent replacement of the 2-phenyl moiety with methyl was of little consequence. These data enhanced our confidence in the preferred binding mode (Fig. 3a) and enabled the initiation of lead optimization.

Concurrent with this work,[10] we were investigating pyridinyl–pyrazole oximes, and were aware that an appropriately positioned oxime moiety, represented by SB-590885[11] and GDC-0879 (Fig. 1),[10] could impart both potency and Raf selectivity. Because the 4-chlorophenyl group of **1b** was modeled to reside in the same region as the oxime moiety of GDC-0879, we opted to explore imidazopyrazine oximes.

Table 1 shows SAR for selected imidazopyrazines. Introduction of the indane–oxime moiety (compare **2b** and **1a**, **1b**) led to a

* Corresponding authors.
E-mail addresses: li.ren@arraybiopharma.com (L. Ren), Ellen.Laird@arraybiopharma.com (E.R. Laird).

0960-894X/$ - see front matter © 2010 Elsevier Ltd. All rights reserved.
doi:10.1016/j.bmcl.2010.12.039

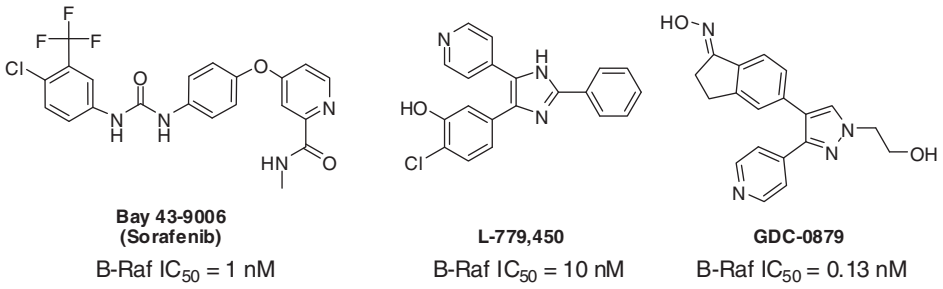

Figure 1. Selected B-Raf inhibitors known at the outset of this work.

significant improvement in enzyme (V600E B-Raf) potency and measurable inhibition of phospho-ERK production. Various substituents (compounds **2a**–**2d**) were tolerated at C2, consistent with our presumed binding mode. It is notable that analogs that are capable of an internal hydrogen bond to the C3 NH (i.e., compounds **2a** and **2d**)[12] showed modest enhancement in enzyme potency, but considerable improvement in the cellular assays. The internal hydrogen bond may provide a conformational constraint to the desired binding mode, and may also mask polar surface area and improve cell permeability.

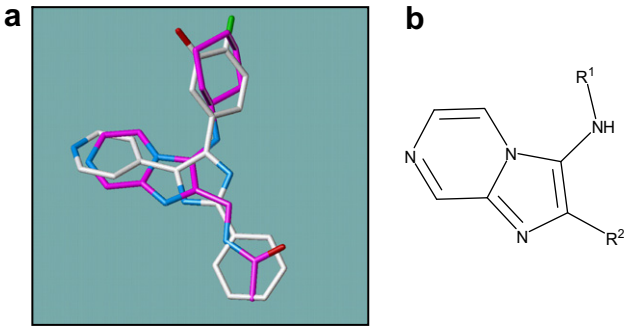

Figure 2. (a) Selected virtual screening hit. The query triarylimidazole (L-779,450) is shown in white, and a representative ROCS virtual screening hit is depicted in magenta. (b) The generic imidazo[1,2-*a*]pyrazine template.

Table 1
Activity of imidazopyrazines

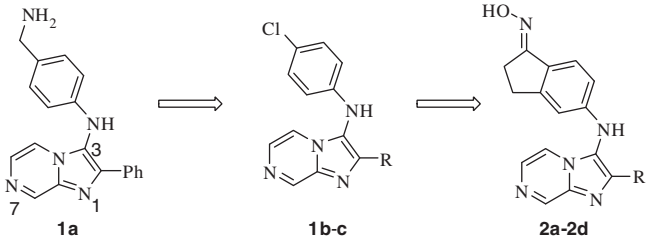

Compound	R	B-Raf[a] IC_{50} (nM)	pERK[a] IC_{50} (nM)
1a	Ph	1400	—
1b	Ph	570	76,000
1c	Me	1200	—
2a	-§-CO_2Et	16	3100
2b	Ph	35	19,000
2c	-§- 	47	16,000
2d	-§- 	4	1400

[a] Biochemical and cellular IC_{50} values are an average of three experiments.

Despite significant improvement in activity for this series, the imidazopyrazines did not approach the level of inhibition attained in the pyridinyl–pyrazole oxime series that was under investigation simultaneously.[10] We hypothesized that this could arise from a number of contributing factors, including differences in conformational energetics, parameters relating to exposed and buried surface area, and hydrogen-bonding capabilities. We determined from conformational profiling at the 6-31G(d) level of theory[13] that, while the bound conformation of the pyridinyl–pyrazole template lies very near its global minimum, the bound conformation of the imidazopyrazines lies ca. 3.4 kcal/mol above the global minimum conformer. In addition, relative to the corresponding pyridinyl–pyrazoles, the total buried surface area for the imidazopyrazines is significantly lower upon engagement by the active site, but the fraction of polar surface area buried is higher (data not shown). This suggests less Van der Waals contact coupled with a potentially higher desolvation penalty.

We evaluated various electronic parameters for alternatives to the imidazopyrazine. Calculation of partial atomic charges and interaction potentials is often used as a measure of hydrogen-bond accepting ability for inhibitors.[14] Figure 4 illustrates these computed properties for several fused templates versus a simplified pyridinyl–pyrazole.

The imidazopyrazine template buries a substantial amount of strongly polar surface area, owing to the significant charge density at N1. On the other hand, the thieno[2,3-*c*]pyridines were predicted to maintain the same overall geometry with improved hydrogen-bond accepting capability for the hinge interaction, and thus comprised our next targets.

A number of thienopyridines were synthesized and representative examples are shown in Table 2. To our satisfaction, the thieno-

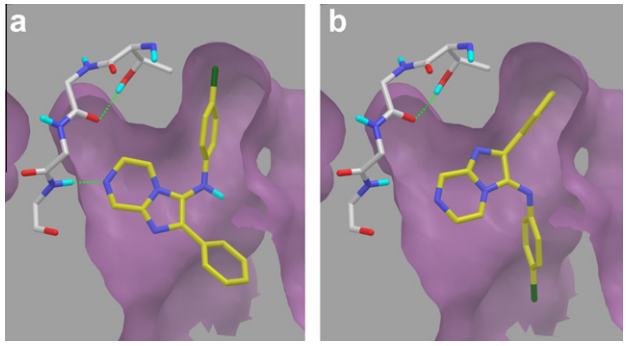

Figure 3. Possible binding modes for compound **1b**.[9] (a) The preferred binding mode, based on evaluation of HTS data (data not shown) and precedence in kinase X-ray structures for halogenated aromatics in the gatekeeper pocket. The distance between N7 and the hinge nitrogen is 2.8 Å. (b) Alternative binding mode; disfavored owing to a nonoptimal hinge contact for N7 (over 3.7 Å) and N1 (over 3.8 Å). The sidechains of the hinge residues are undisplayed for clarity; the sidechain of the gatekeeper (Thr529) is explicitly illustrated. Hydrogen-bonding interactions are illustrated with dashed green lines.

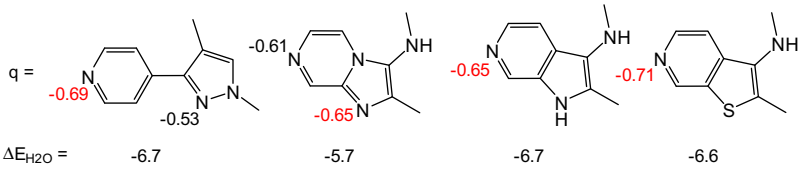

Figure 4. Electronic properties for B-Raf templates. q = computed partial atomic charges labeled on potential hydrogen-bond accepting atoms; red labeling highlights the atom of highest negative charge. ChelpG charges were computed for structures that were optimized using the 6-31G(d) basis set. ΔE_{H2O} is the computed interaction potential with water as a general donor for the hinge-acceptor atom.[15] Note that the thienopyridine template has a partial charge on the hinge-binding acceptor atom that closely resembles that of the potent pyridinyl–pyrazole, and was hence the template of choice.

Table 2
Representative thienopyridines

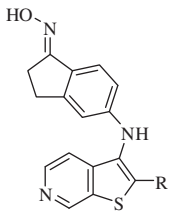

3a-3g

Compound	R	B-Raf[a] IC_{50} (nM)	pERK[a] IC_{50} (nM)
3a	-CO$_2$Et	3	280
3b	-CONMe$_2$	40	5800
3c	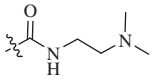	52	8200
3d	H	32	7300
3e	Ph	3	1500
3f		3	170
3g	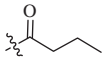	<2[b]	140

[a] Biochemical and cellular IC_{50} values are an average of three experiments.
[b] IC_{50} value below the detection limit of the routine enzyme assay.

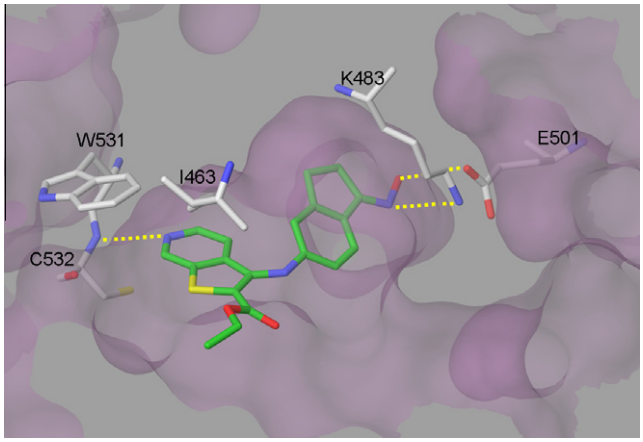

Figure 5. X-ray crystal structure of thienopyridine **3a** bound to B-Raf. Hydrogen bonds are depicted as dashed yellow lines, and include interactions with the mainchain NH of Cys532 of the hinge sequence, and contacts between the oxime OH and Glu501 and the oxime nitrogen with Lys483. Evaluation of Van der Waals contacts reveals that the sulfur atom makes significant contact to the sidechain of Ile463.

pyridines did show significant improvements in both enzyme and cellular potencies (compare **2a** and **3a**, **2b** and **3e**, and **2c** and **3f**). Shortly after we began investigating this series, the first X-ray crystal structures of imidazopyrazines and thienopyridines were solved. Figure 5 illustrates the X-ray structure of **3a**,[16] and also reveals that the thienopyridines have additional hydrophobic contacts to Ile463 of the P-loop, which probably also contributes to the enhanced potency.

In spite of the improved activity of the thienopyridines, a drawback of this series was its propensity to inhibit multiple CYP P450s at sub-micromolar concentrations, possibly via mechanisms related to the well-known metabolic activation of thiophene moieties.[17] For example, IC_{50} values of **3a** for CYP3A4, 2C19, and 1A2 were determined to be 50, 129, and 616 nM, respectively.

The inherent CYP liabilities of the thienopyridines suggested a core change was necessary and we opted to address this issue by substituting the sulfur with oxygen;[18] several of the resulting

Table 3
Representative furopyridines

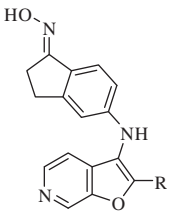

4a-4h

Compound	R	B-Raf[a] IC_{50} (nM)	pERK[a] IC_{50} nM
4a	-CO$_2$Et	<2[b]	30
4b	-CONMe$_2$	5	340
4c	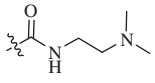	2	40
4d	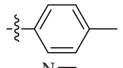	3	2000
4e		<2[b]	150
4f		<2[b]	960
4g	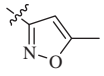	<2[b]	365
4h		0.2[c]	5

[a] Biochemical and cellular IC_{50} values are an average of three experiments.
[b] IC_{50} value below the detection limit of the routine enzyme assay.
[c] The enzyme IC_{50} of **4h** was determined in a more sensitive assay using a lower concentration of the B-Raf protein.

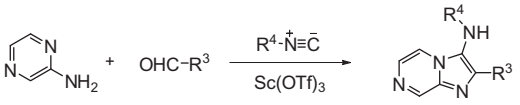

Scheme 1. Preparation of imidazopyrazines.

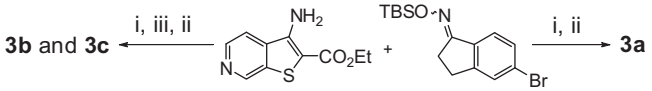

Scheme 2. General synthesis of thienopyridines **3a**–**3c**: (i) $Pd_2(dba)_3$, XPhos, Cs_2CO_3, toluene, 110 °C, (75%); (ii) TFA, (89%); (iii) HNR_1R_2, Me_3Al, (80%).

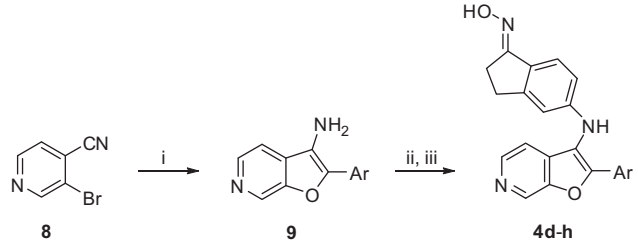

Scheme 4. Synthesis of 2-aryl and 2-heteroarylfuropyridines: (i) NaH, $ArCH_2OH$, DMF, −10 °C, 30 min; then **8**, 60 °C, 16 h (35%); (ii) 5-bromo-2,3-dihydroinden-1-one *O*-*tert*-butyldimethylsilyl oxime, $Pd_2(dba)_3$, XPhos, Cs_2CO_3, toluene, 110 °C, (70%); (iii) TBAF, THF, (90%).

furo[2,3-*c*]pyridines[19] are shown in Table 3. The first compound synthesized was ethyl ester **4a**, which was superior to both its corresponding imidazopyrazine and thienopyridine analogs (**2a** and **3a**, respectively) in terms of enzyme and cellular potency. Furthermore, furopyridine ester **4a** exhibited a much improved P450 profile: IC_{50} values for CYP3A4, 2C19 and 1A2 were 8300, 1177 and >25,000 nM, respectively.

Encouraged by these results and in an effort to improve the chemical and metabolic stability of the series, we synthesized several amides (represented by **4b** and **4c**) and found that secondary amides were superior to tertiary amides. Amide **4c** displayed improved aqueous solubility (>1 mg/mL at pH 6.5), high caco-2 permeability, and low predicted clearance from human and rodent hepatocytes. We also examined the placement of various aryl and heteroaryl groups at the 2-position. Aryl derivatives (exemplified by **4d**) in general were less potent in cell assays, but heteroaryl derivatives showed striking differences in cellular potency depending on substitution. For example, 3-pyridyl derivative **4f** showed improvement over **4d**, but was inferior to 2-pyridyl derivative **4e**. As we had observed for the imidazopyrazines, superior cellular activity appeared to correlate with the ability to form an internal hydrogen bond, with concomitant masking of polar surface area. When a second nitrogen atom was incorporated into the pyridine ring system (exemplied by pyrimidine **4h**), the result was an extremely potent B-Raf inhibitor that exhibited a picomolar IC_{50} in the V600E biochemical assay and corresponding low nanomolar inhibition of pERK. Overall, we regarded the furopyridine series to be superior to the thienopyridines and imidazopyrazines owing to its clean P450 profile and potent in vitro activity.

The imidazopyrazine scaffold was rapidly constructed via a 3-component, 4+1 cyclization reaction[20] involving an aldehyde, 2-aminopyrazine, and an isonitrile in the presence of scandium triflate (Scheme 1). In most cases, the oximes were isolated as a mixture of both the *E*- and the *Z*-isomer, with the *E* being the predominant form (>9:1 *E*/*Z* ratio). In several cases, we were able to separate the *E*, *Z* isomers by column chromatography; the *E* isomers were typically five-fold more active in both enzyme and cell assays.

Table 4
ADME properties of selected furopyridine analogs

Compound	Hepat. Cl[a]	Caco-2[b]	Pe ratio	Sol. @ pH 6.5
4c	17	High	0.9	>1000
4h	28	High	0.9	2

[a] Rat hepatocyte clearance (ml/min/kg).
[b] Caco-2 permeability classification: low (<2×10^{-6} cm/s), medium (2–8×10^{-6} cm/s), high (>8×10^{-6} cm/s).

Thienopyridine esters and amides (**3a**–**3c**) were synthesized according to Scheme 2. Ethyl 3-aminothieno[2,3-*c*]pyridine-2-carboxylate[21] was used in a Buchwald coupling with 5-bromo-2,3-dihydro-1*H*-inden-1-one *O*-*tert*-butyldimethylsilyl oxime[22] to form the critical NH linkage. Silyl deprotection then afforded ester **3a** directly. Amides **3b** and **3c** were prepared by treating the silyl protected ester with preformed amino aluminates, followed by removal of the sily protecting group.

For the 2-aryl- and 2-heteroarylthienopyridines (**3e**–**3f**), the method of LaMattina and Taylor[23] was used to construct the requisite 2-arylthieno[2,3-*c*]pyridin-3-amine. Subsequent XPhos-mediated palladium coupling with 5-bromo-2,3-dihydro-1*H*-inden-1-one *O*-*tert*-butyldimethylsilyl oxime followed by silyl deprotection afforded the desired 2-aryl thienopyridines. The 2-keto derivatives (**3g**) were constructed via the Weinreb amide.[19]

The preparation of furopyridine esters and amides is outlined in Scheme 3. Ethyl 3-hydroxyfuro[2,3-*c*]pyridine-2-carboxylate (**6**) has been reported previously,[24] however, in our hands the reported alkylation of ethyl 3-hydroxyisonicotinate (**5**) with ethyl 2-bromoacetate was problematic in that we consistently observed large amounts of byproduct resulting from alkylation on the pyridine nitrogen. In order to avoid the undesired alkylation, this transformation was carried out under Mitsunobu conditions and the desired product was isolated in consistently higher yields. Subsequent cyclization to **6** was accomplished in excellent yield using NaH. The hydroxyl group was then converted to the corresponding triflate and a Buchwald coupling afforded ester **7**. Amides **4b** and

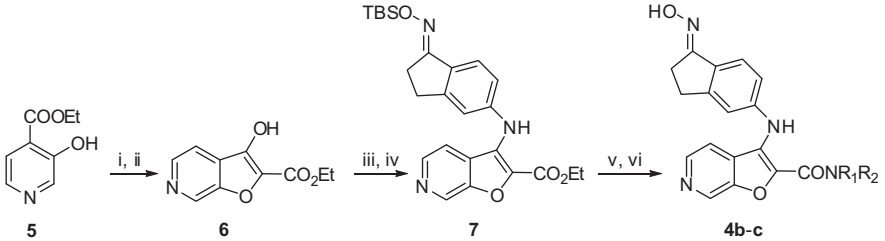

Scheme 3. Synthesis of amide furopyridines **4b**–**4c**: (i) PPh_3, DIAD, −10 °C, 30 min; then ethyl glycolate, −10 °C, 30 min; then **5**, −10 °C to room temperature (76%); (ii) NaH, THF, 0 °C to room temperature, then HOAc (84%); (iii) Tf_2O, Py, DCM (90%); (iv) 5-amino-2,3-dihydroinden-1-one *O*-tert-butyldimethylsilyl oxime, $Pd_2(dba)_3$, XantPhos, K_3PO_4, toluene, 110 °C, (70%); (v) NHR_1R_2, $AlMe_3$, 0 °C, 30 min; then **7**, (vi) TBAF, THF.

4c were generated by reacting **7** with preformed amino aluminates followed by removal of the silyl protecting group.[19]

2-Aryl-3-amino furopyridines (**9**) were prepared from 3-bromoisonicotinonitrile **8** according to the procedure of LaMattina and Taylor.[23] The subsequent transformations to **4d**–**4h** were similar to the thienopyridine series and are highlighted in Scheme 4.

Being of interest due to its cellular activity, **4h** was screened against a panel of 25 non-RAF kinases at 1 μM. Satisfyingly, **4h** did not show greater than 50% inhibition against any of the enzymes with the exception of casein kinase 1 delta.

The in vitro ADME and pharmacokinetic profiles of furopyridines **4c** and **4h** were determined. Although **4c** and **4h** were found to be intrinsically stable in plasma and in liver hepatocytes, and were highly permeable without efflux (Table 4), both compounds were rapidly cleared from the plasma compartment when dosed in rats (data not shown). The in vivo/in vitro disconnection can be partially explained by the poor stability of **4h** in rat microsomes (CL_{pred} = 50 ml/min/kg). Degradation of the oxime moiety to the corresponding ketone was hypothesized and can occur via well-known CYP mediated processes as well as in the presence of stomach acid.[25] This possibility led to a significant effort toward the identification of indazole-based B-raf inhibitors, which we describe in the following paper.[26]

Via virtual and high-throughput screening we discovered an imidazopyrazine template as a lead structure for inhibition of B-Raf. X-ray crystal structures confirmed the expected binding mode, and consideration of binding orientation and electronic properties enabled optimization to thienopyridines as a more potent second-generation lead. Optimization of the thienopyridines to remove the inherent CYP liabilities eventually led us to the highly potent furopyridines, of which several potent and selective B-RAF inhibitors have been identified. In the following paper, we describe further evolution of the series geared toward enhanced pharmacokinetic properties.

Acknowledgment

The authors thank Susan Rhodes, Jennifer Otten, and Michelle Livingston for Caco, P450, and solubility determinations. The authors also thank Drs. Joachim Rudolph and Stefan Gradl for critical review of the manuscript and helpful suggestions.

References and notes

1. (a) Davies, H.; Bignell, G. R.; Cox, C.; Stephens, P.; Edkins, S.; Clegg, S.; Teague, J.; Woffendin, H.; Garnett, M. J.; Bottomley, W., et al *Nature* **2002**, *417*, 949; (b) Beeram, M.; Patnaik, A.; Rowinsky, E. K. *J. Clin. Oncol.* **2005**, *23*, 6771; (c) Dhillon, A. S.; Kolch, W. *Cancer Cell* **2004**, *5*, 303.
2. (a) Ramurthy, S.; Subramanian, S.; Aikawa, M.; Amiri, P., et al *J. Med. Chem.* **2008**, *51*, 7049; (b) Eisen, T.; Ahmad, T.; Flaherty, K. T.; Gore, M.; Kaye, S.; Marias, R., et al *Br. J. Cancer* **2006**, *95*, 581.
3. Heimbrook, D. C.; Huber, H. E.; Stirdivant, S. M.; Patrick, D. R.; Claremon, D.; Liverton, N.; Selnick, H.; Ahern, J.; Conroy, R.; Drakas, R.; Falconi, N.; Hancock, P.; Robinson, R.; Smith, G.; Olif, A. American Association for Cancer Research, New Orleans, Apr 1998; Poster #3793.
4. *ROCS*: OpenEye Scientific Software: Santa Fe, NM. Virtual hits were comprised of compounds from a 50% sampling of our focused library collection (approximately 200,000 virtual compounds) with a purely shape-matching Tanimoto index of 0.85 or more.
5. Laird, E.; Topalov, G.; Lyssikatos, J. P.; Welch, M.; Grina, J.; Hansen, J.; Newhouse, B. WO 2006125101.
6. For assay description see: Laird, E.; Lyssikatos, J.; Welch, M.; Grina, J.; Hansen, J.; Newhouse, B.; Olivero, A.; Topolav, G. WO 2006/084015 A2, 2006.
7. The homology model was constructed using the program COMPOSER (Tripos Associates, St. Louis MO). The X-ray coordinates of Lck in complex with PP2 (PDB accession code 1QPE) were chosen as the major template.
8. Noble, M. E. M.; Endicott, J. A.; Johnson, L. N. *Science* **2004**, *303*, 1800.
9. Binding modes were generated using the program GOLD (v2.2) Jones, G.; Willett, P.; Glen, R. C.; Leach, A. R.; Taylor, R. *J. Mol. Biol.* **1997**, *267*, 727.
10. Hansen, J. D.; Grina, J.; Newhouse, B.; Welch, M.; Topalov, G.; Littman, N.; Callejo, M.; Gloor, S.; Martinson, M.; Laird, E.; Brandhuber, B. J.; Vigers, G.; Morales, T.; Woessner, R.; Randolph, N.; Lyssikatos, J.; Olivero, O. *Bioorg. Med. Chem. Lett.* **2008**, *28*, 4692.
11. Takle, A. K.; Brown, M. J. B.; Davies, S.; Dean, D. K.; Francis, G.; Gaiba, A.; Hird, A. W.; King, F. D.; Lovell, P. K.; Naylor, A.; Reith, A. D.; Steadman, J. G.; Wilson, D. M. *Bioorg. Med. Chem. Lett.* **2006**, *16*, 378.
12. The existence of an internal hydrogen bond was later confirmed by X-ray crystallography. Vide infra.
13. Gaussian98, Revision A.11. Frisch, M.J. et al. Gaussian Inc. Pittsburgh PA.
14. (a) Murray, J. S.; Ranganathan, S.; Politzer, P. *J. Org. Chem.* **1991**, *56*, 3734; (b) Chan, A. W. E.; Golec, J. M. C. *Bioorg. Med. Chem.* **1996**, *4*, 1673; (c) McClure, K. F.; Abramov, Y. A.; Laird, E. R.; Barberia, J. T.; Cai, W.; Carty, T. J.; Cortina, S. R.; Danley, D. E.; Dipesa, A. J.; Donahue, K. M.; Dombroski, M. A.; Elliott, N. C.; Gabel, C. A.; Han, S.; Hynes, T. R.; LeMotte, P. K.; Mansour, M. N.; Marr, E. S.; Letavic, M. A.; Pandit, J.; Ripin, D. B.; Sweeney, F. J.; Tan, D.; Tao, Y. *J. Med. Chem.* **2005**, *48*, 5728.
15. Interaction potentials were the averaged energy for a water molecule interacting with the hinge acceptor of the inhibitor as computed via Monte Carlo simulation using the OPLS potential function and the TIP4P water model: (a) Jorgensen, W. L.; Tirado-Rives, J. *J. Am. Chem. Soc.* **1988**, *110*, 1657; (b) Jorgensen, W. L.; Blake, J. F.; Buckner, K. *Chem. Phys.* **1989**, *129*, 193.
16. Coordinates for the B-Raf crystal structure have been deposited in the PDB: accession code 3PSB.
17. Dalvie, D. K.; Kalgutkar, A. S.; Khojasteh-Bakht, S. C.; Obach, R. S.; O'Donnell, J. P. *Chem. Res. Toxicol.* **2002**, *15*, 269.
18. Calculation of partial atomic charges for the furopyridine template resulted in −0.67 for the pyridyl nitrogen.
19. Miknis, G.; Lyssikatos, J. P.; Laird, E.; Tarlton, E.; Buckmelter, A. J.; Ren, L.; Rast, B.; Schlachter, S. T.; Wenglowsky, S. M. US 2007049603.
20. (a) Groebke, K.; Weber, L.; Mehlin, F. *Synlett* **1998**, 661; (b) Blackburn, C.; Guan, B.; Fleming, P.; Shiosaki, K.; Tsai, S. *Tetrahedron Lett.* **1998**, *39*, 3635; (c) Bienayme, H.; Bouzid, K. *Angew. Chem., Int. Ed.* **1998**, *37*, 2234.
21. Beugelmans, R.; Bois-Choussy, M.; Boudet, B. *Tetrahedron* **1983**, *39*, 4153.
22. 5-Bromo-2,3-dihydro-1*H*-inden-1-one *O*-*tert*-butyldimethylsilyl oxime was synthesized in 99% yield by heating 5-bromo-2,3-dihydro-1*H*-inden-1-one and NH_2OTBS in the presence of a catalytic amount of TsOH.
23. LaMattina, J. L.; Taylor, R. L. *J. Org. Chem.* **1981**, *46*, 4179.
24. Morita, H.; Shiotani, S. *J. Heterocycl. Chem.* **1986**, *23*, 549.
25. (a) Kumpulainen, H.; Mähönen, N.; Laitinen, M.-L.; Jaurakkajärvi, M.; Raunio, H.; Juvonen, R. O.; Vepsäläinen, J.; Järvinen, T.; Rautio, J. *J. Med. Chem.* **2006**, *49*, 1207; (b) Heberling, S.; Girreser, U.; Wolf, S.; Clement, B. *Biochem. Pharmacol.* **2006**, *71*, 354.
26. Ren, L.; Wenglowsky, S.; Miknis, G.; Rast, B.; Buckmelter, A. J.; Ely, R. J.; Schalachter, S.; Laird, E. R.; Randolph, N.; Callejo, M.; Martinson, M.; Galbrainth, S.; Brandhuber, B. J.; Viger, G.; Voegtli, W. C.; Morales, T.; Lyssikatos, J. *Bioorg. Med. Chem. Lett.* **2011**, *21*, 1243.